International Journal of Fatigue 166 (2023) 107279

Contents lists available at ScienceDirect

International Journal of Fatigue

journal homepage: www.elsevier.com/locate/ijfatigue

Fatigue crack characterisation in 2024-T351 aluminium alloy through SEM observation combined with the CJP model

J.M. Robles [a], J.M. Vasco-Olmo [b], A.S. Cruces [a,*], F.A. Diaz [b], M.N. James [c,d], P. Lopez-Crespo [a,*]

[a] Department of Civil and Materials Engineering, University of Malaga, C/Dr Ortiz Ramos, s/n, 29071 Malaga, Spain
[b] Departamento de Ingeniería Mecánica y Minera, Escuela Politécnica Superior de Jaén, Universidad de Jaén, Spain
[c] School of Engineering, Computing & Mathematics, University of Plymouth, Plymouth, UK
[d] Department of Mechanical Engineering, Nelson Mandela University, Port Elizabeth, South Africa

ARTICLE INFO

Keywords:
Fatigue crack growth
CJP model
Digital Image Correlation
Scanning Electron Microscopy

ABSTRACT

This work characterises crack growth in AA2024-T315 by combining different methods to further increase the reliability of the results. The Christopher-James-Patterson (CJP) model was fitted to experimental data obtained by digital image correlation (DIC). The effective value of the CJP stress intensity factors were successfully correlated with the ΔK-da/dN curve as obtained with Scanning Electron Microscopy measurements of the depth of striations on the fracture surface. This approach based on fitting the CJP model with DIC data and SEM observations allowed estimation of opening and closure loads and allowed the propagation rate and fracture mode to be effectively characterised.

1. Introduction

Currently, large catastrophic fatigue failures, which can result in high losses in both economic terms and human life, continue to occur in many industries. In fact, fatigue is the most important cause of failure in metallic materials [1]. It is now well known that crack growth is impacted by many different effects, one of the most important of which is plasticity-induced crack tip shielding, also described as crack closure. This phenomenon has triggered a great deal of controversy, as the actual effect on propagation and the best way to measure crack closure is not known for certain [2,3].

Paris' relationship [4] is the basis for many fatigue studies, though a number of limitations of the da/dN-ΔK equation have been pointed out in the last 50 years. Certain authors, such as Walker [5] or Forman [6], proposed variations of the model in order to consider different effects, including the effect of the stress rate (R) or the maximum stress intensity factor, that impact the crack growth rate; while other new models are even being proposed that substitute the Paris law, such as the Crack Tip Opening Displacement (CTOD)-based models [7]. It is in this context that the CJP model, developed using the Muskhelishvili complex potential method was created [8]. Some studies have demonstrated the versatility of the method through different analysis of the four parameters obtained from it [9]: K_F, which is similar to the traditional mode I stress intensity factor (SIF), but with certain formulation differences that account for shielding aspects [10]; a retardation stress intensity factor, K_R; a shear stress intensity factor, K_S and the *T*-stress. This model has proven to have enhanced accuracy in characterising plasticity zone size and shape and crack growth rate data when plasticity-induced shielding is present [11], compared with the use of the Paris equation and the usual effective range of SIF. The CJP model facilitates full field analysis of stress, strain and displacement at the tip of a fatigue crack [12]. Moreover, this method can avoid the complex calculation of plastic strains, because it focuses on calculating the stress field acting at the elasto-plastic boundary [13]. Nowadays, the possibility of combining CTOD and CJP models is being considered to better understand plasticity-induced crack tip shielding [14].

The information collected from the fracture surface has been previously used to infer essential information regarding the fatigue process. For example Forsyth [15] showed the correlation of striations and the advance of the crack in one cycle and Fleck [16] established that this relationship is logarithmic with the SIF range. Numerous studies conducted to date, including Hertzberg [17] work, have observed a relationship between these striations and the crack closure effect and related the depth of the mark with the load level. Other researchers have found a relationship between different striations on the fracture surface and the crack closure effect, such as the presence of secondary cracks [18],

* Corresponding authors.
E-mail addresses: ascruces@uma.es (A.S. Cruces), plopezcrespo@uma.es (P. Lopez-Crespo).

https://doi.org/10.1016/j.ijfatigue.2022.107279
Received 6 April 2022; Received in revised form 13 September 2022; Accepted 15 September 2022
Available online 21 September 2022

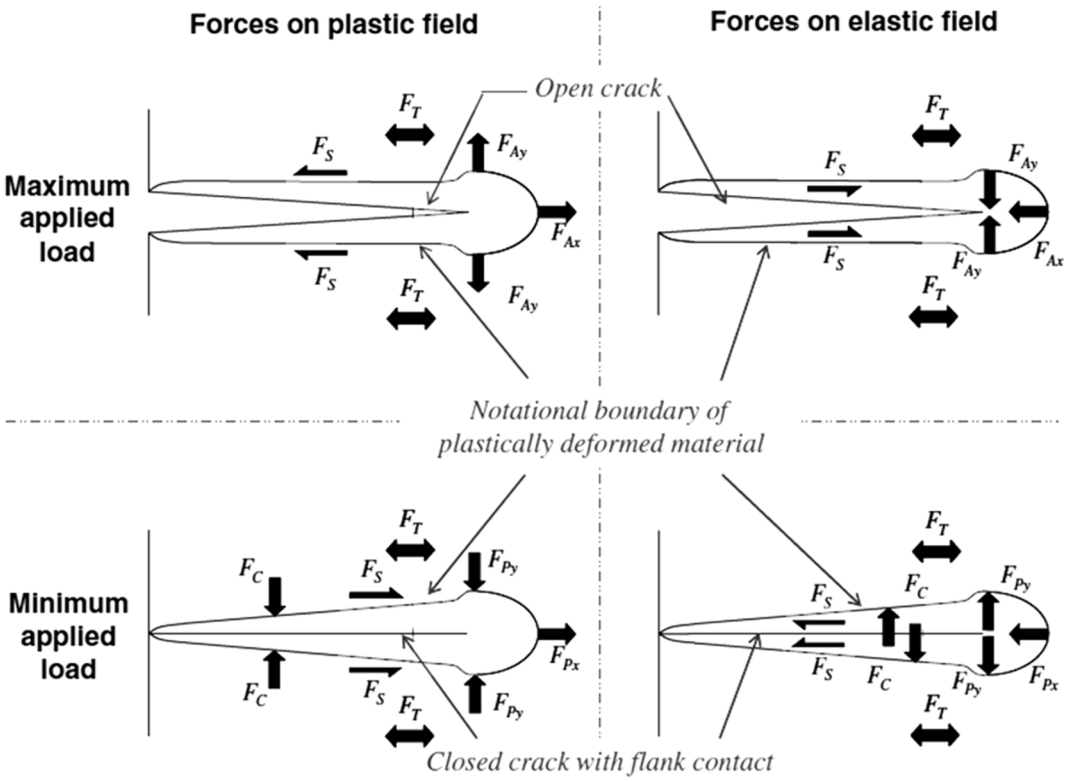

Fig. 1. Schematic of the forces acting at the interface of the plastic zone and the surrounding elastic material.

smearing or relatively rough surfaces [19,20]. In summary, SEM analysis of the fracture surface can facilitate observation of crack growth and crack closure.

This paper, therefore, combines two different fatigue methods to characterise the fatigue crack propagation behaviour of a 2024 aluminium alloy, namely SEM observations of the fracture surface and the powerful CJP model to characterise the plastic enclave surrounding the crack, taking into account the contact forces and the compatibility-induced shear stress. This is done by retrieving propagation data from the CJP model and analysing its correlation with the Paris law information obtained through the observation of the fracture surface with SEM. This is one of the very few studies that makes use of a traditional materials science approach to fatigue analysis combined with a global approach based on continuum mechanics.

2. Theoretical principles

2.1. CJP model

The CJP model is used in this work to characterise crack growth. The method involves calculating the displacement fields with DIC and using this information to determine the new SIFs that incorporate the effects of plasticity-induced shielding that are defined in this model. The model hypothesis is that the plastic enclave surrounding the fatigue crack tip extends along its flanks and will partially protect the crack from the applied elastic stress field through both crack flank contact forces effect ("crack closure" along the wake of the crack) and the interfacial shear stress induced by the compatibility at the elastic–plastic boundary. James et al. [21] provided a schematic idealisation of the forces repeated here as Fig. 1, which illustrates the forces believed to act at the interface between the plastic zone and the surrounding elastic material. The parameters obtained from this method can be explained by the forces shown in Fig. 1, and the displacement fields were characterised in the model as:

$$\begin{aligned} 2G(u+iv) =& \kappa\left[-2(B+2E)z^{\frac{1}{2}}+4Ez^{\frac{1}{2}}-2Ez^{\frac{1}{2}}\ln(z)-\frac{C-F}{4}z\right] \\ & -z\left[-(B+2E)\overline{z}^{\frac{1}{2}}-E\overline{z}^{\frac{1}{2}}\overline{\ln(z)}-\frac{(C-F)}{4}\right] \\ & -\left[A\overline{z}^{\frac{1}{2}}+D\overline{z}^{\frac{1}{2}}\overline{\ln(z)}-2D\overline{z}^{\frac{1}{2}}+\frac{C+F}{2}\overline{z}\right] \end{aligned} \quad (1)$$

In equation (1), G represents the shear modulus, κ is a parameter that acquires a different value in case of plane stress (κ=(3-ν)/(1 + ν)) or plane strain (κ = 3-4ν), ν is Poisson's ratio and coefficients A, B, C, D, E and F define the displacement fields around the crack front.

The opening mode stress intensity factor K_F is defined using the same remote loading as the traditional K_I parameter, but is modified due to the force components that are derived from the stress components presented at the elasto-plastic boundary, which influence the driving force. Thus, unlike the classical stress intensity factor K_I, K_F includes additionally the plasticity-induced crack shielding effects and is identical with K_I as long as no shielding effect takes place. K_F is defined from the asymptotic limit of σ_y as $x \to +0$, along $y = 0$, that is towards the crack tip in the crack plane ahead of the crack:

$$K_F = \lim_{r\to 0}\left[\sqrt{22\pi r}\left(\sigma_y + 2Er^{\left(-\frac{1}{2}\right)}\ln(r)\right)\right] = \sqrt{\frac{\pi}{2}}(A-3B-8E) \quad (2)$$

1. The retardation stress intensity factor K_R characterises the forces applied in the crack plane and provides a retardation effect on fatigue crack growth. K_R is then evaluated from σ_x in the limit as $x \to -0$, along $y = 0$, that is towards the tip the crack and along the crack flank:

$$K_R = \lim_{r\to 0}[\sqrt[2]{2\pi r}\sigma_x] = -(2\pi)^{\frac{3}{2}}E \quad (3)$$

Table 1
Main properties of Aluminium alloy 2024-T351 [30].

Ultimate tensile strength (MPa)	Tensile yield strength (*MPa*)	Elongation in 50 mm (%)	Brinell Hardness (HB)	Ultimate shearing strength (MPa)	Fatigue endurance limit (MPa)	Modulus of elasticity (GPa)	Poisson's ratio
485	345	18	120	285	140	73	0.33

2. K_S characterises the compatibility-induced shear stress along the crack plane at the interface between the plastic enclave and the surrounding elastic field and is derived from the asymptotic limit of σ_{xy} as $\times \rightarrow$ -0, along y = 0, that is towards the crack tip along the crack wake:

$$K_S = \lim_{r\to 0}[\sqrt[2]{2\pi r}\sigma_{xy}] = \pm\sqrt{\frac{\pi}{2}}(A+B) \tag{4}$$

3. F_T depicted in Fig. 1 occurs due to *T*-stress. *T*-stress is defined by two components: Tx on the x-axis and Ty on the y-axis, the equation of each component being:

$$T_x = -C$$

$$T_y = -F \tag{5}$$

2.2. Crack closure effect

The crack closure effect is central to this paper because the study specimen exhibits this effect, which is characterised by its impact on fatigue crack growth. Elber [22] assumed that fatigue cracks must be open in order to propagate. In the case of a crack closure effect, such as in the present study, in which the maximum and minimum loads are both positive, the effective range of load during which the crack is open is reduced compared with the applied load range, due to various effects such as roughness [23], oxidation [24] or induced deformations [25] that arise from residual stresses.

In this way, the calculation of the effective SIF factor can be expressed as shown in equation (6), instead of the one used if the effect is not present (equation (7)), and the Paris equation can be defined as shown in equation (8).

$$\Delta K_{eff} = K_{max} - K_{op} \tag{6}$$

$$\Delta K_{nom} = K_{max} - K_{min} \tag{7}$$

$$\frac{da}{dN} = C\hat{A}\cdot(K_{max} - K_{op})^m \tag{8}$$

In these equations, C and m are constants that depend on the test and the material, K_{max} is the SIF for the maximum load and K_{op} is the SIF for the load at which the crack tip actually opens. Additionally, a parameter to quantify this crack closure effect called the crack closure ratio (U), defined by equation (9), was proposed by Elber.

$$U = \frac{K_{max} - K_{op}}{K_{max} - K_{min}} \tag{9}$$

The main controversy currently being discussed in the literature is on how to obtain the value of ΔK_{eff} with which the ratio between U and R or other mechanical parameters could be obtained. Numerous studies have demonstrated the inverse relationship between U and R, since increasing R reduces the value of U; for example, Elber [22] established a linear relationship between them by performing experiments with some aluminium alloys. Newman [26] established a non-linear relationship between both parameters. However, some authors such as Walker [27] or De Koning [28] believe that this effect is not only related to R, but also depends on other factors such as K_{max}, ΔK, σ_{ys}, and some others. Currently, researchers are also studying more complex models, or the relationship with other parameters such as the one proposed by Zhang [29], which considers the variation of crack closure as well as the opening load combined with the effect of some external factors that impact crack growth. In the present paper we shall apply the effective SIF found via the CJP model.

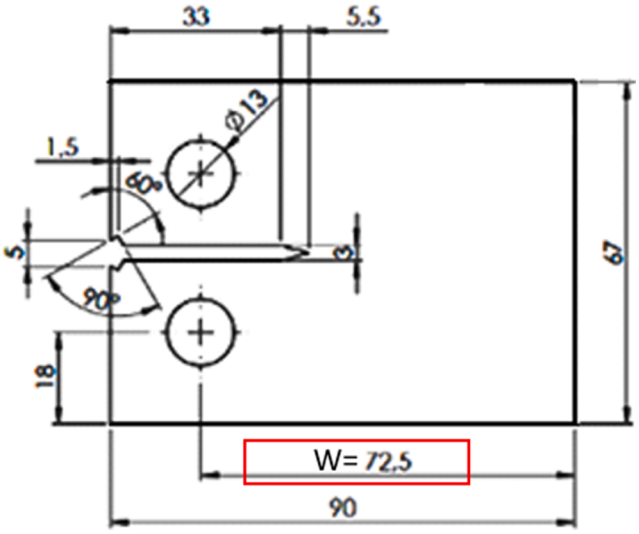

Fig. 2. Geometry of the specimen and measurement of the W value highlighted.

3. Material and specimen analysed

The material studied in this work was aluminium alloy 2024-T351. This aluminium alloy has a wide variety of applications, especially in aeronautics industry. In this case, a specimen was extracted from a 2 mm sheet of material and a Compact Tension (CT) sample was machined from it.

The widespread use of this alloy is mainly due to its good mechanical properties, combining high mechanical strength with low weight and good ductility. The main mechanical properties of 2024-T351 alloy can be seen in Table 1.

This type of alloy obtains its properties by the combination of the S-phase (Al_2CuMg), Guinier-Preston-Bagaryatsky zones and other different groups of precipitates. When hot-fabricated, dispersoid and *T*-orthorhombic phase precipitates can also be present [31].

4. Experimental procedure

4.1. Test procedure

Testing was performed using a servo-hydraulic MTS370.10 machine capable of applying a maximum load of 100kN with a frequency of 10 Hz. The test was performed with a load ratio (R) of 0.008 with a minimum load of 5 N and maximum load of 600 N.

The test frequency was slowed down to 0.005 Hz periodically to take photographs throughout a loading cycle, for DIC analysis of the full-field displacement and strain. The geometry of the specimens used in this study is shown in Fig. 2.

4.2. DIC procedure and equipment

The DIC technique was used to determine the displacement fields

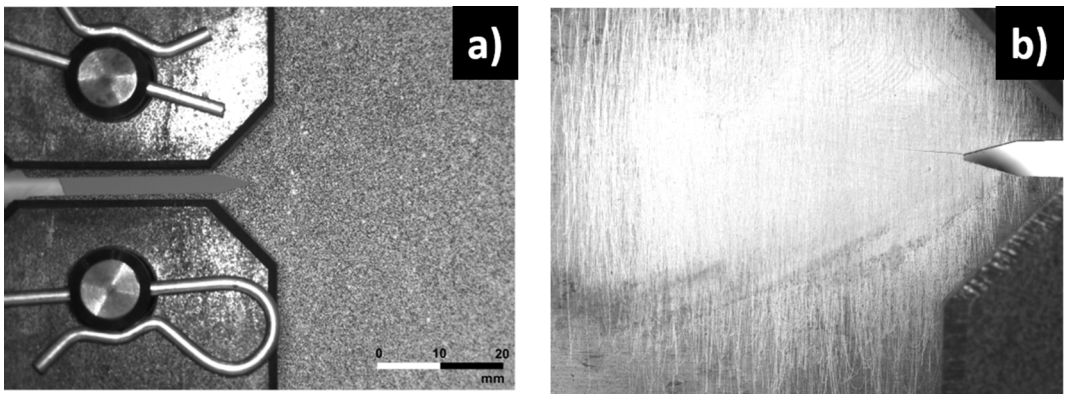

Fig. 3. a) Pattern used in CT specimen for DIC and b) Pattern used for crack tracking [32].

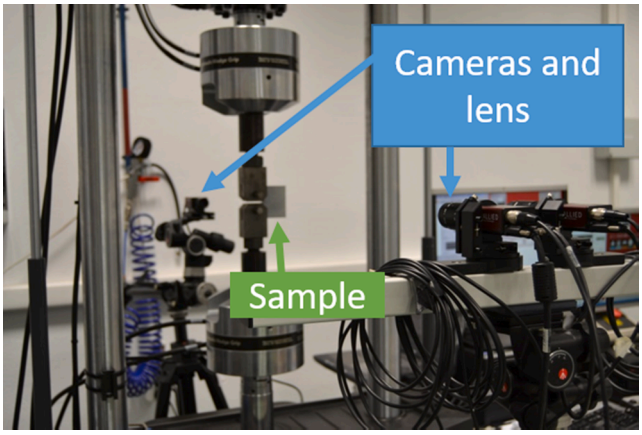

Fig. 4. Camera and sample setup.

used in subsequent calculation of stresses and strains. For this purpose, different treatments were applied to either side of the sample. One side of the surface was sprayed to obtain a white background pattern with randomly-distributed small black dots, and was used for the DIC work, as shown in Fig. 3a. The other side was ground and polished, as shown in Fig. 3b, so as to be able to track the crack growth on it.

Once the samples were prepared a two CCD camera set-up was used. Each camera, equipped with a 75 mm lens, was placed perpendicular to one side of the sample, as shown in Fig. 4. During fatigue testing, a Stingray F-504B/C camera was employed for image capturing. This camera has a CCD progressive as sensor type, a sensor size type 2/3 and a resolution of 2452x2056 pixels. In terms of DIC, vic-2D software, developed by Correlated Solutions company was used to obtain the displacement fields.

For the camera imaging the DIC pattern it was ensured that crack path was located in the central part of the image, giving the results illustrated in Fig. 5.

The multipoint over-deterministic method that was developed by Sanford and Dally [33] was used to obtain the various stress intensity factors. The method is only valid in the elastic zone near the crack front, therefore this zone must be defined to obtain valid experimental data. This leads to the use of an annular mesh of measurement points, as shown in Fig. 5, with an inner radius large enough so as to avoid including the plastically deformed zone and an outer radius that is inside the region dominated by the crack tip elastic stresses. The size of the inner radius was determined by estimating the extent of plastic deformation at the crack tip, applying the Von Mises yield criterion to establish the region around the crack tip in which the stress values exceed the yield stress [34]. However, the vertical displacement fields were used to establish the required size of the outer radius, by observing the field orientation change caused by the interaction between the region dominated by the crack front and the region dominated by the specimen edge effects.

4.3. SEM process to characterise crack growth

Numerous materials science analyses have used SEM, and in this case it will be used to characterise crack growth through fatigue striation observation. A JEOL JSM 840 microscope was used, it was not equipped

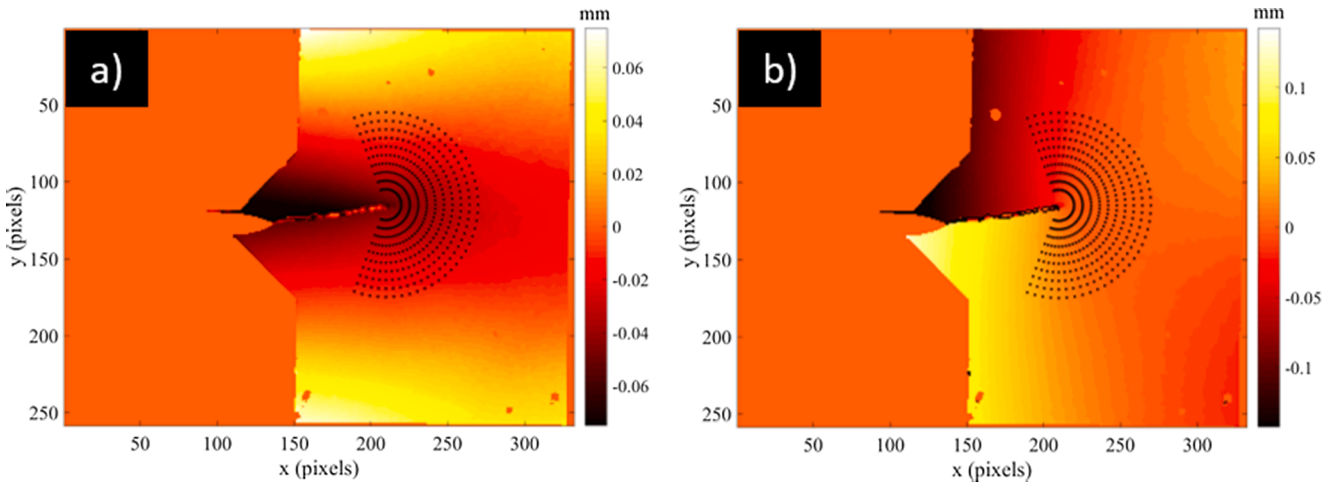

Fig. 5. Vertical (a) and horizontal (b) displacement fields for a crack length of 37.6 mm.

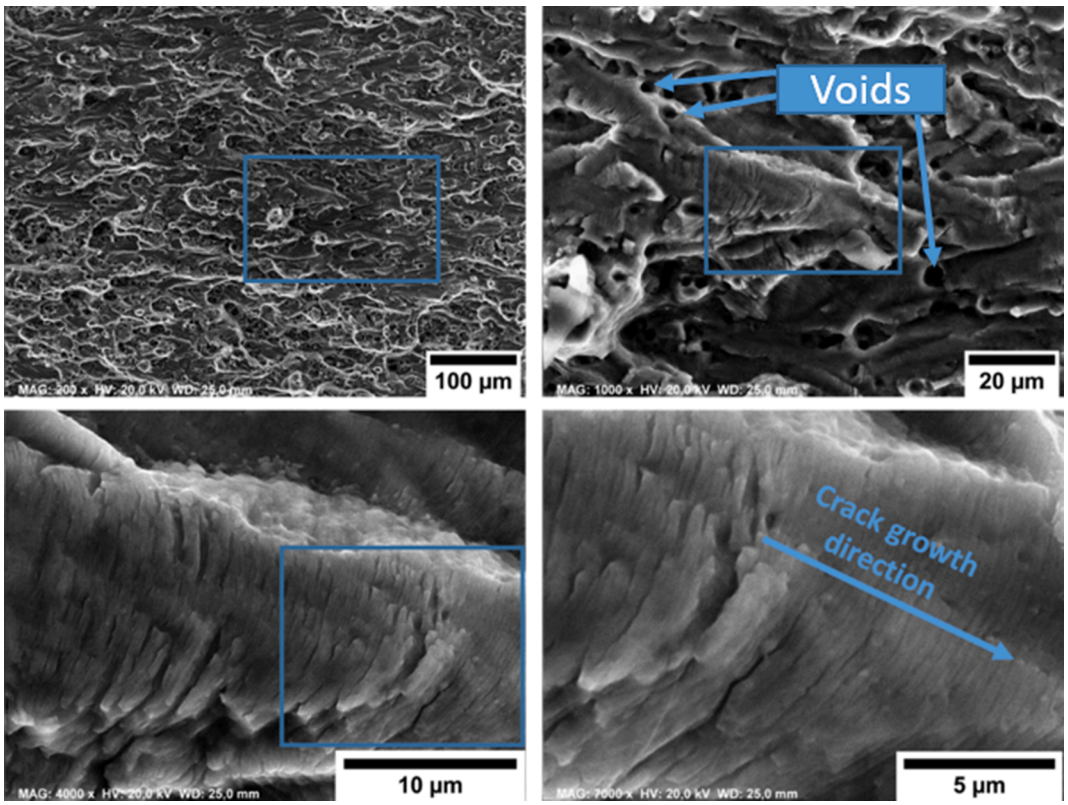

Fig. 6. Gradual approach to the area where striations are detected.

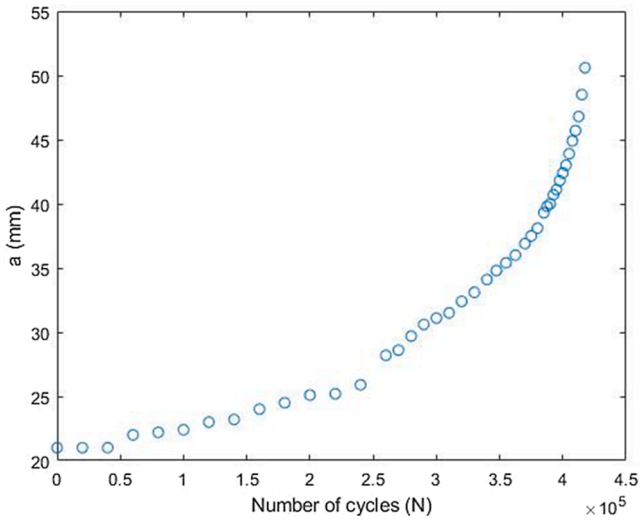

Fig. 7. Crack growth as a function of the number of cycles, a given in mm.

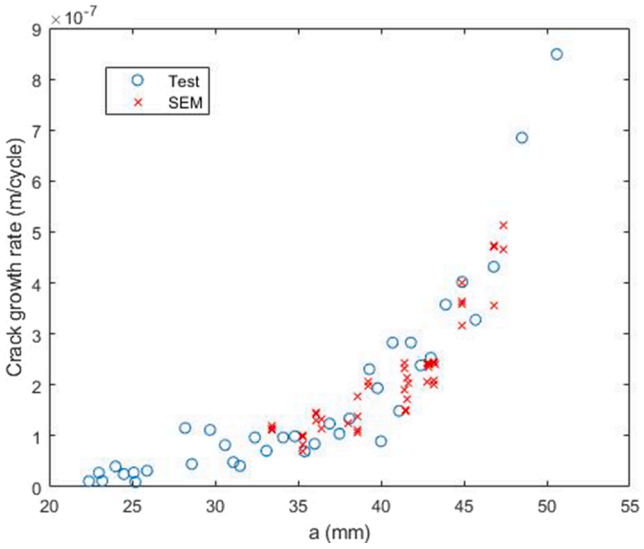

Fig. 8. Comparison between the data obtained with SEM and during the a vs da/dN test.

with a FEM. The detector, which was employed to capture the images, was a SE detector and the spot size used was 15 nm. The process consists of the following steps:

1. First, the sample is loaded on the microscope stage and the microscope parameters are calibrated to ensure that the fracture surface can be viewed properly.
2. With the sample in place, the fatigue striations are located and brought into focus until they are close enough to accurately measure the distance between them, as shown in Fig. 6.
3. Next, the distance between the striations must be measured perpendicular to the striations, and in this study ImageJ software [35] was used for this purpose. Fig. 6 shows a large number of fatigue striations in a specific area, and the distance between them is calculated by taking several measurements and taking the average of all of them. This gives the value of the local crack growth rate, da/dN, for a given crack length.
4. The last step, after calculating the distances between the striations, is to obtain the stress intensity factors (SIFs) as per ASTM [36] in order to characterise the crack growth and plot the Paris curves. Fig. 3 shows the geometry used and equation (10) is the one proposed by the ASTM to obtain the SIF through the data obtained from SEM.

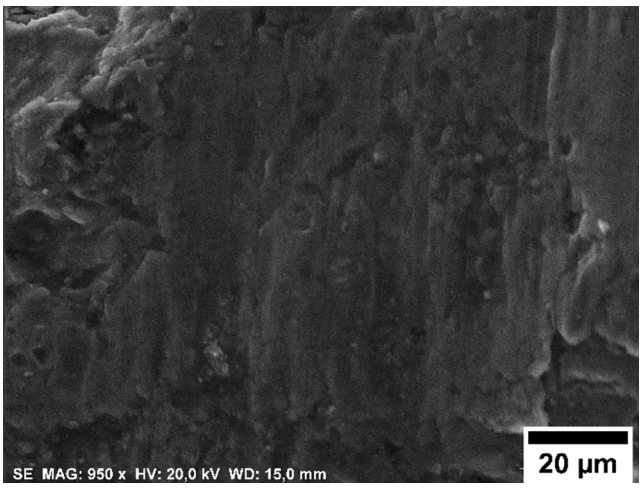

Fig. 9. SEM image of different zones of the threshold and near start of the crack growth.

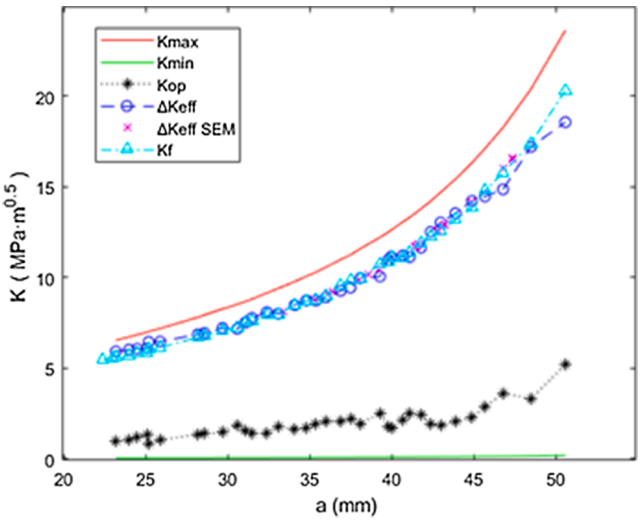

Fig. 11. SIF values as a function of crack length.

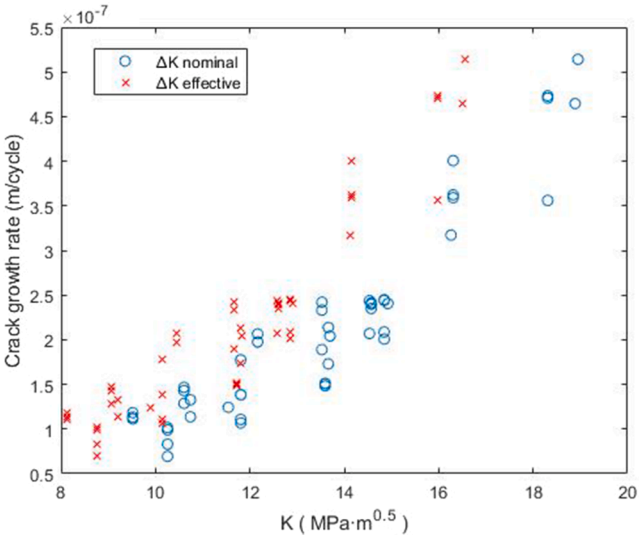

Fig. 10. Paris curves for both the effective and nominal values of the SIF.

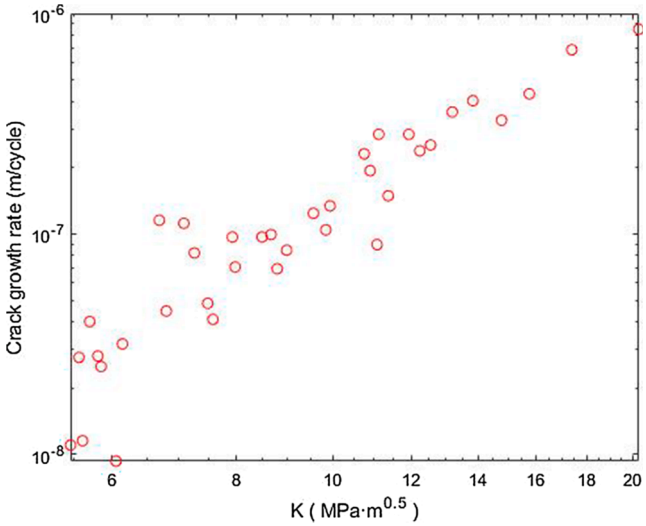

Fig. 12. Crack growth rate data obtained with the CJP model, using the K_F parameter versus da/dN.

$$\Delta K = \frac{\Delta P \hat{A} \cdot f}{t \hat{A} \cdot \left(\frac{W}{1000}\right)^{0.5}} \tag{10}$$

4.4. Experimental results

A long distance microscope was used throughout the test to observe and monitor the crack length with increasing number of cycles. This crack length evolution is shown in Fig. 7.

Taking into account the test data and to check that the data obtained with SEM were accurate, Fig. 8 plots the crack growth rate (da/dN) at different crack lengths. Fig. 8 compares the crack propagation rates obtained with the two different methodologies, namely, travelling microscope and distance between fatigue striations (SEM). Fig. 8 shows a good correlation between both sets of data.

Fig. 8 indicates that the data obtained via SEM measurement is accurate over the range of data studied, i.e. a crack length exceeding 35 mm. It was complicated measuring cracks less than 35 mm long due to the state of the sample, which was a darker, greyer colour. Furthermore, the striations were closer together, making it harder to measure the distances between them. Fig. 9 displays an SEM image of the threshold zone where no striation measurements were made due to poor surface condition and vertical wear. The poor condition of the sample in this area was probably due to the humidity and environmental conditions that is likely to produce fretting oxidation and deterioration of the surface, through contact between the crack faces.

Fig. 6 clearly shows voids in the fracture surface. These voids are indicative of fracture behaviour being ductile. SEM analysis also showed evidence of the crack closure effect, such as the appearance of smooth surfaces [1920] due to contact and friction between the faces or the appearance of secondary cracks linked to this contact [37]. Both features are characteristic of crack closure.

Once the SIFs for the different points have been determined, the Paris curve was obtained, from the da/dN measurements with SEM, by determining the change in da/dN with respect to ΔK at the different points. Fig. 10 shows both the effective and nominal SIF values, where both the opening and closing loads were calculated from the offset compliance method [38,39].

Equation (6) was used to calculate the effective values, while equation (7) was used for the nominal values. Fig. 10 shows a clear difference between the effective and nominal SIF values, providing a clear indication of a considerable crack closure effect.

In this particular case, the opening load was used to calculate the

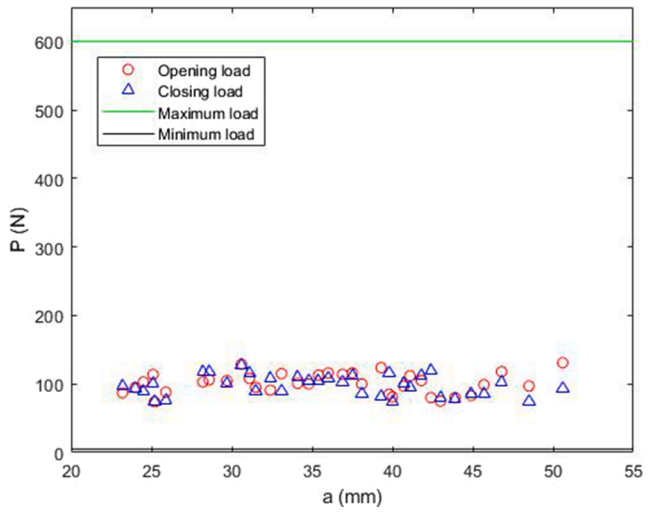

Fig. 13. Opening and closing loads along the crack length obtained by K_F analysis.

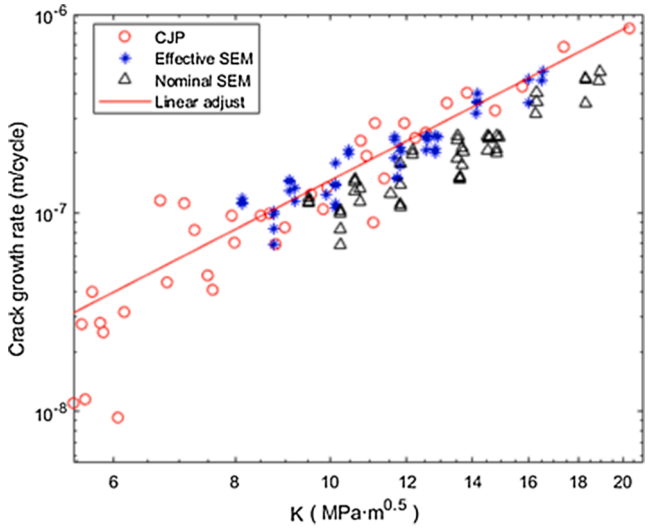

Fig. 14. Comparison between Paris law curves obtained by CJP and SEM (nominal and effective values).

ΔK_{eff}. This is supported by Moreno's findings focused on the load range studied in the current work [41]. It is worth noting than in some cases (e.g. short cracks) the influence of the stress ratio [40,42] and the difference between opening and closing loads may be large enough to be considered. Fig. 11 shows the correlation between the K_{eff} data obtained with equation (6) for different crack lengths and the K_{eff} obtained by SEM.

Fig. 11 plots SIF values as a function of crack length and also shows corresponding values of K_{op}, K_{max} and K_{min}. It is clear that ΔK_{eff} is less that the range of $K_{max} - K_{min}$. Similarly, the SIF values obtained by SEM can be seen to correlate accurately with the experimentally calculated effective SIF values when considering the opening load obtained with the compliance offset method [14].

The CJP model was also used to characterise crack growth with the displacement field data calculated by DIC. Fig. 12 shows the Paris curve using K_F obtained by CJP for the study specimen.

In addition, analysing the evolution of the K_F parameter during different loading cycles during the test provided the K_{op} and K_{cl} parameters, which would be the opening and closing stress intensity factors. These can be used to calculate the opening and closing load by

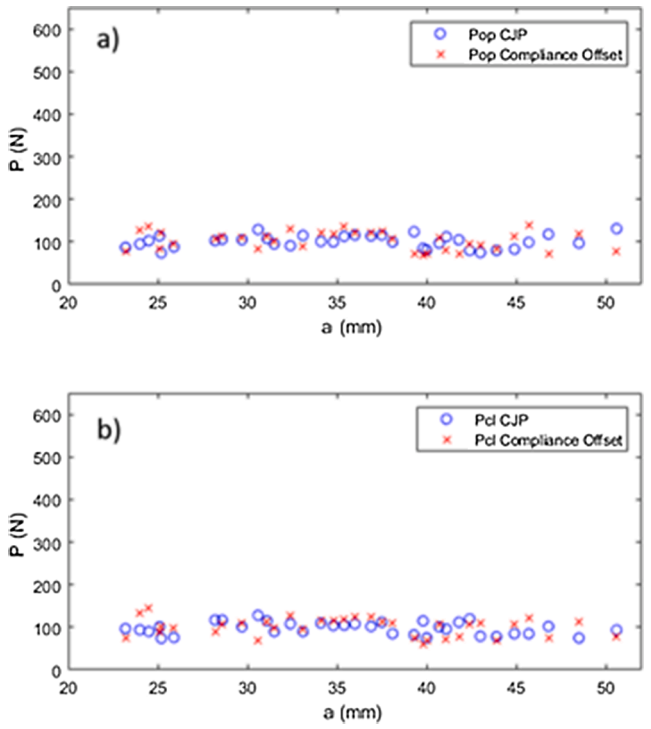

Fig. 15. Evolution of the opening (a) and closing (b) loads along the crack obtained by both CJP and compliance offset.

applying equation (11), but instead of using ΔK, K_{op} and K_{cl} are used to calculate P_{op} and P_{cl} respectively. Fig. 13 shows the closing and opening loads along the crack length obtained by CJP.

As shown in Figs. 12 and 13, the CJP model was used to conduct a study similar to the experimental crack growth study, and K_F parameter provided the Paris curves that characterise the crack growth and the opening and closing loads, which have a direct effect on it.

This section compares and analyses the data obtained using the CJP method and the experimental data obtained with DIC, compliance offset or SEM. First of all, the correlation between the Paris curve data obtained by SEM and CJP, which can be seen in Fig. 14, will be analysed.

Fig. 14 compares the CJP crack growth data with the nominal and effective SEM data. Due to the scattering of the data produced for the methods, especially for the data obtained from SEM, the analysis was carried out with a large number of points that allowed improved statistics. The larger scattering observed in SEM data is caused by the higher level of measurement which is more influenced by the microstructure. On the contrary, the scattering is lower when measuring at the macroscopic level. The scattering of the data from CJP can be observed mainly at the beginning, this first zone of crack growth has a different behaviour, due to the effect of the microstructure and the microstructural barriers [43].

To estimate the quality of the correlation, a statistical study of both growth curves was carried out, performing a linear regression to obtain the C and m values that define the Paris curve, shown in equation (11). The curve approximated by the linear regression was the one obtained by CJP, giving a C parameter value of $4.30 \cdot 10^{-10}$ and an m parameter of 2.53. The correlation between both methods was evaluated with the r^2 parameter, which is calculated with equation (11):

$$r^2 = 1 - \frac{\sum (y_i - \widetilde{y_i})^2}{(\sum y_i^2) - \frac{(\sum y_i)^2}{n}} \tag{11}$$

Where n is the number of points to evaluate, y_i are the experimental values obtained by SEM and $\widetilde{y_i}$ are the fitted curve values obtained by calculating the C and m parameters. When the CJP data were compared

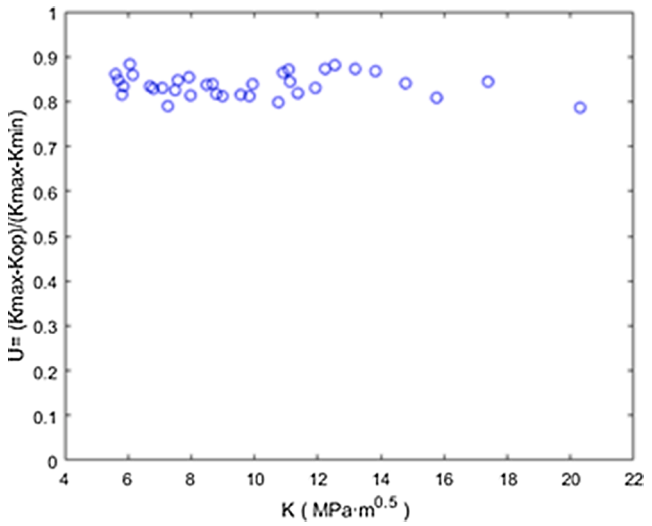

Fig. 16. Evaluation of the U parameter as the SIF increases.

with the effective SEM data, the r^2 value obtained was 0.94, while upon comparison with the nominal SEM data, the r^2 value was negative, indicating a poor correlation [44]. Thus, it could be established that the KF data obtained by CJP are close to the effective data obtained by SEM, indicating that the CJP model can capture the effect of crack closure in characterising fatigue crack growth. Upon comparison with other studies, characterising crack growth with the CJP model for 2024 aluminium can be seen to give a better approximation than with other models such as those studied by Kumar [45]. For comparison purposes, the degree of correlation of Kumar models was also evaluated on the same specimen, material and load ratio, with r^2 values in the range of [0.64–0.89]. This suggests that the CJP fitting shown here produces a lower scattering and thus a better fitting. This is supported by the works from Yang [46], where the best correlation was observed for the CJP model. Hence, it appears that CJP model enables a more accurate characterisation of the displacement field at the crack front, conducting a comparative study of the CJP model with three other models (Westergaard, Williams and Muskhelishvili), and also provides additional information of interest, as suggested previously [39].

Furthermore, in order to validate the data obtained by CJP, a comparative study was performed of the opening (Fig. 15a) and closing (Fig. 15b) load data obtained with CJP, through KF analysis and those obtained by the compliance offset method.

An analysis of Fig. 15, which displays the superposition of the opening load (Fig. 15a) and closing load (Fig. 15b) data, shows no notable difference between the data obtained by CJP and by the compliance offset method, reflecting a similar accuracy in both methods.

The crack closure effect was quantified using the U parameter, currently-one of the most accepted and used for this purpose. Its evolution for the different effective SIF calculated is represented in Fig. 16.

The crack closure data obtained in Fig. 16 were observed and compared with the simulations carried out by Garcia-Collado [47], in which crack growth was simulated with conditions practically identical to those used in this paper. In both cases, the U-parameter was observed to be in the same range as those obtained in this study. Higher values of crack closure were expected, since the larger plastic zone meant that a bigger portion of the volume yielded, thus producing lower values of U [48]. Nevertheless, the closure levels measured here are roughly in agreement with other previous works focused also on plane stress conditions [49,50,47]. It would be interesting to extend the current analysis to plane strain conditions. It was also seen that the U-parameter tends not to grow with increasing SIF value under these conditions.

5. Conclusions

In this work, an experimental characterisation of fatigue crack growth for 2024-T351 aluminium alloy has been performed. Two different optical techniques have been used, SEM and DIC. To the authors' knowledge, it is the first time that microstructure data obtained by SEM and experimental data obtained from the analysis of crack tip displacement fields measured by DIC are combined to characterise fatigue crack growth through such a robust model, on a particularly relevant material to the aerospace industry due to its high strength and good resistance to fatigue propagation. For the study using DIC, the CJP model has been used for the characterisation of crack tip displacement fields due to its demonstrated ability to incorporate the shielding effects of the plastic enclave on a growing fatigue crack [51]. In the present work, the trend of *KF* throughout a full loading cycle was followed and it should be noted that this is not the same as the value of ΔK_{CJP}, defined by Yang [46]. In the case of the study by SEM, the crack length was measured from an exhaustive analysis of the fracture surface. Therefore, the experimental results obtained with the CJP model has been linked to the fatigue crack growth rates obtained from the fracture observation with SEM. In addition, ductile fracture with large accumulation of voids was observed by SEM. These voids have special importance in the first stage of the growth, where they can act like microstructural barriers and reduce the crack growth rate. Beyond this initial stage, the main mechanism is the conventional fatigue crack growth through striations. However, the ductile behaviour exhibited can produce a significant plastic enclave and plastic zone around the crack tip, which in turn also influences crack closure. Moreover, several evidences of the crack closure effect were observed on the microscope, in agreement with the retardation effects observed through CJP model, these evidences are shown in the Fig. 17, where smooth surfaces [19] and secondary cracks

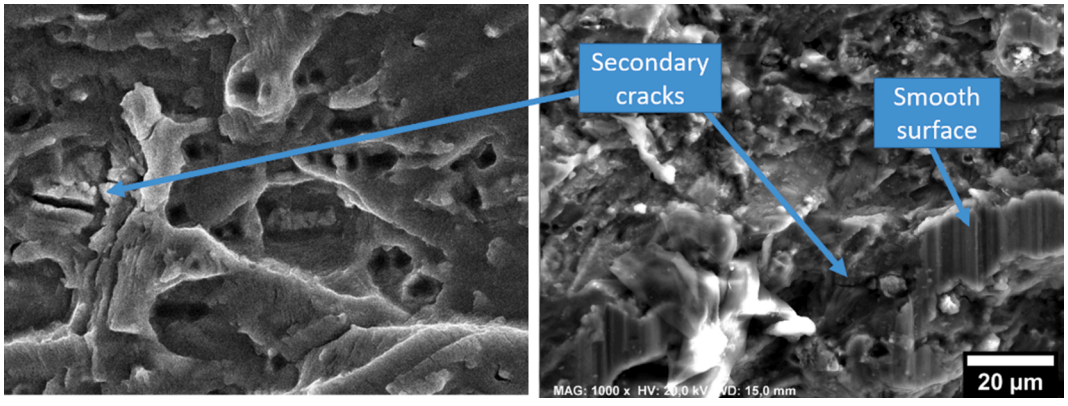

Fig. 17. Evidences of the crack closure on the fracture surface.

[18] can be observed, which are produced due to the contact between the faces during the fatigue test. The shielding effect induced by the plastic enclave generated around the crack during crack propagation was clearly noticeable. These evidences can also be observed in the fracture surface through the different marks (striations) created by the contact of the faces. The load analysis during a cycle let to appreciate the opening retardation for a higher load value to the minimum load, which is a strong indicative of crack closure.

This work has demonstrated that it is possible to characterise fatigue crack growth by combining experimental data acquired by DIC during fatigue tests using DIC with crack measurements obtained from the fracture analysis by SEM.

Declaration of Competing Interest

The authors declare that they have no known competing financial interests or personal relationships that could have appeared to influence the work reported in this paper.

Data availability

Data will be made available on request.

Acknowledgements

The authors would like to acknowledge the financial support of Programa Operativo FEDER from the Junta de Andalucia (Spain) through grant reference UMA18-FEDERJA-250. Industrial support from Bettergy SL and from Dr N Ordonez and M Carrera is also greatly acknowledged, as well as access to different components and materials in the energy industry. The authors would also like to acknowledge the financial support from Junta de Andalucia through the research project "1380786" funded by the program "Proyectos de I + D + I en el Marco del Programa Operativo FEDER Andalucia 2014-2020. Convocatoria 2020." We would also like to acknowledge funding for open access charge: Universidad de Malaga / CBUA

References

[1] Callister WD. Materials science and engineering: an introduction. 7th ed. New York: Jonh Wiley & Sons; 2007.
[2] James M. Some unresolved issues with fatigue crack closure - measurement, mechanisms and interpretation problems, Advances in Fracture Research. Proc Ninth Int Conf Fract 1996:5.
[3] Stoychev S, Kujawski D. Methods for crack opening load and crack tip shielding determination: A review. Fatigue Fract Eng Mater Struct 2003;26:1053–67.
[4] Paris P, Erdogan F. A Critical Analysis of Crack Propagation Laws. J Basic Eng 1963;85:528–33.
[5] Walker K. The Effect of Stress Ratio During Crack Propagation and Fatigue for 2024–T3 and 7075–T6 Aluminum. Eff Environ Complex Load Hist Fatigue Life, STP 462. Am Soc Test Mater 1970;1:1–14.
[6] Forman RG, Kearney VE, Engle RM. Numerical Analysis of Crack Propagation in Cyclic-Loaded Structures. J Basic Eng 1967;89:459–63.
[7] Antunes FV, Branco R, Prates PA, Borrego L. Fatigue crack growth modelling based on CTOD for the 7050–T6 alloy. Fatigue Fract Engng Mater Struct 2017;40:1309–20.
[8] Muskhelishvili NI. Some Basic Problems of the Mathematical Theory of Elasticity. Groningen: Noordhoff International Publishing; 1977.
[9] Olmo JMV, Garrido FAD, Vicente RD, García RL. Comparativa de modelos para el cálculo experimental del factor de intensificación de tensiones empleando técnicas ópticas de campo completo. Asoc Española Ing Mecánica 2011.
[10] James MN, Christopher CJ, Lu Y, Tee KF, Patterson EA. Crack tip shielding from a plastic "inclusion". Key Eng Mater 2011;465:1–8.
[11] Vasco-Olmo JM, Díaz FA, Patterson EA. Experimental evaluation of shielding effect on growing fatigue cracks under overloads using ESPI. Int J Fatigue 2016;83(2):117–26.
[12] James MN, Vasco-Olmo JM, Díaz FA, Antunes FV, Bing Y, Huang Y. Characterisation of fatigue crack growth using the CJP model of crack tip fields or plastic CTOD. Procedia Struct Integr 2019;23:613–9.
[13] Vasco-Olmo JM, Díaz FA. Experimental evaluation of plasticity-induced crack shielding from isochromatic data. Opt Eng 2015;54.
[14] Vasco-Olmo JM, Díaz FA, Antunes FV, James MN. Characterisation of fatigue crack growth using digital image correlation measurements of plastic CTOD. Theor Appl Fract Mech 2019;101:332–41.
[15] Forsyth PJE, Ryder DA. Fatigue Fracture, Some Results Derived from the Microscopic Examination of Crack Surfaces. Aircr Eng 1960;32:96–9.
[16] Fleck NA, Smith RA. Effect of density on tensile strength, fracture toughness, and fatigue crack propagation behaviour of sintered steel. Powder Metall 1981;24:121–5.
[17] Hertzberg RW, Von EE. Crack closure and fatigue striations in 2024–T3 aluminum alloy 1973;4:887–9.
[18] Okayasua M, Chenb D, Wanga Z. Experimental study of the effect of loading conditionon fracture surface contact features and crackclosure behavior in a carbon steel. Eng Fract Mech 2006:1117–32.
[19] Fratini L, Pasta S, Reynolds AP. Fatigue crack growth in 2024–T351 friction stir welded joints: Longitudinal residual stress and microstructural effects. Int J Fatigue 2009;31:495–500.
[20] Hu Y, Cheng H, Yu J, Yao Z. An experimental study on crack closure induced by laser peening in pre-cracked aluminum alloy 2024–T351 and fatigue life extension. Int J Fatigue 2020;130:105232.
[21] James MN, Christopher CJ, Lu Y, Patterson EA. Local crack plasticity and its influences on the global elastic stress field. Int J Fatigue 2013;46:4–15.
[22] Elber W. Fatigue Crack Closure Under Cyclic Tension. Eng Fract Mech 1970;2:37–44.
[23] Kim JH, Lee SB. Behavior of plasticity-induced crack closure and roughness-induced crack closure in aluminum alloy. Int J Fatigue 2001;23:247–51.
[24] Suresh S, Zamiski GF, Ritchie DRO. Oxide-Induced Crack Closure: An Explanation for Near-Threshold Corrosion Fatigue Crack Growth Behavior. Metall Mater Trans A 1981;12:1435–43.
[25] Curtis S, De Los Rios ER, Rodopoulos CA, Levers A. Analysis of the effects of controlled shot peening on fatigue damage of high strength aluminium alloys. Int J Fatigue 2002;25:59–66.
[26] Newman J. A Finite-Element Analysis of Fatigue Crack Closure. Mech. Crack Growth, 100 Barr Harbor Drive, PO Box C700, West Conshohocken, PA 19428-2959: ASTM International; n.d., p. 281-281–21.
[27] Walker N, Beevers CJ. A fatigue crack closure mechanism in titanium. Fatigue Fract Eng Mater Struct 1979;1:135–48.
[28] de Koning A. A Simple Crack Closure Model for Prediction of Fatigue Crack Growth Rates Under Variable-Amplitude Loading. Fract. Mech., 100 Barr Harbor Drive, PO Box C700, West Conshohocken, PA 19428-2959: ASTM International; n.d., p. 63-63–23.
[29] Zhang P, Xie L qi, Zhou C yu, Li J, He X hua. Two new models of fatigue crack growth rate based on driving force parameter and crack closure method at negative load ratios. Theor Appl Fract Mech 2019;103.
[30] ASM Metals Handbook - Properties and selection nonferrous alloys and special purpose- Volume 2. 1996.
[31] Sha G, Marceau RKW, Gao X, Muddle BC, Ringer SP. Nanostructure of aluminium alloy 2024: Segregation, clustering and precipitation processes. Acta Mater 2011;59:1659–70.
[32] Olmo JMV. Experimental evaluation of plasticity induced crack shielding effect using full-field optical techniques for stress and strain measurement PhD student. Universidad de Jaén 2014.
[33] Sanford RJ, Dally JW. A general method for determining mixed-mode stress intensity factors from isochromatic fringe patterns. Eng Fract Mech 1979;11:621–33.
[34] Vasco-Olmo JM, Diaz FA, James MN, Christopher CJ, Patterson EA. Experimental methodology for the quantification of crack tip plastic zone and shape from the analysis of displacement fields. Frat Ed Integrità Strutt 2017;11:166–74.
[35] ImageJ n.d. https://imagej.nih.gov/ij/ (accessed July 1, 2021).
[36] ASTM-E1820: Standard Test Method for Measurement of Fracture Toughness 2001:1–46.
[37] Zhou B, Cui H, Liu H, Li Y, Liu G, Li S, et al. Experimental Investigation and Finite Element Analysis on Fatigue Behavior of Aluminum Alloy 7050 Single-Lap Joints. J Mater Eng Perform 2018;27:915–23.
[38] Il CY, Song JH. Improvement of ASTM compliance offset method for precise determination of crack opening load. Int J Fatigue 2009;31:809–19.
[39] Vasco-Olmo JM, Díaz FA, García-Collado A, Dorado-Vicente R. Experimental evaluation of crack shielding during fatigue crack growth using digital image correlation. Fatigue Fract Eng Mater Struct 2015;38:223–37.

[40] Savaidis G, Seeger T. An experimental study on the opening and closure behaviour of fatigue surface, corner and through-thickness cracks at notches. Fatigue Fract Eng Mater Struct 1994;17:1343–56.
[41] Zapatero J, Moreno B, González-Herrera A. Fatigue crack closure determination by means of finite element analysis. Eng Fract Mech 2008;75:41–57.
[42] Sehitoglu H. Crack opening and closure in fatigue. Eng Fract Mech 1985;21:329–39.
[43] Vallellano C, Vázquez J, Navarro A, Domínguez J. A micromechanical model for small fatigue crack growth: An approach based on two threshold conditions. Fatigue Fract Eng Mater Struct 2009;32:515–24.
[44] Everitt BS. The Cambridge dictionary of statistics. 2nd ed. Cambridge, UK: Cambridge University Press; 2003.
[45] Kumar A, Murthy ARC, R.Iyer N. A Study of the Stress Ratio Effects on Fatigue Crack Growth using LOWESS Regression. Int Conf Adv Civil, Struct Andm Eng 2013:47–51.
[46] Yang B, Vasco-Olmo JM, Díaz FA, James MN. A more effective rationalisation of fatigue crack growth rate data for various specimen geometries and stress ratios using the CJP model. Int J Fatigue 2018;114:189–97.
[47] García-Collado A, Vasco-Olmo JM, Díaz FA. Numerical analysis of plasticity induced crack closure based on an irreversible cohesive zone model. Theor Appl Fract Mech 2017;89:52–62.
[48] Borges MF, Lopez-Crespo P, Antunes FV, Moreno B, Prates P, Camas D, et al. Fatigue crack propagation analysis in 2024–T351 aluminium alloy using nonlinear parameters. Int J Fatigue 2021;153:106478.
[49] Borrego LP, Ferreira JM, Costa JM. Fatigue crack growth and crack closure in an AlMgSi alloy. Fatigue Fract Eng Mater Struct 2001;24:255–65.
[50] Borrego LP, Costa JM, Ferreira JM. Fatigue crack growth in thin aluminium alloy sheets under loading sequences with periodic overloads. Thin-Walled Struct 2005;43:772–88.
[51] Christopher CJ, James MN, Patterson EA, Tee KF. Towards a new model of crack tip stress fields. Int J Fract 2007;148:361–71.